JOURNAL OF PROPULSION AND POWER
Vol. 27, No. 4, July–August 2011

Background Pressure Effects on Ion Velocity Distribution Within a Medium-Power Hall Thruster

Michael R. Nakles*
ERC, Inc., Edwards Air Force Base, California 93524
and
William A. Hargus Jr.†
U.S. Air Force Research Laboratory, Edwards Air Force Base, California 93524

DOI: 10.2514/1.48027

An experiment was conducted to study the effects of chamber background pressure on the ion axial velocity distribution within the acceleration channel and the near-field plume of a 600 W xenon Hall effect thruster. Ion velocity distributions were measured along the acceleration channel centerline from the near-anode region to 10 mm downstream of the exit plane using laser-induced fluorescence of the $5d[4]_{7/2} - 6p[3]_{5/2}$ xenon ion excited state transition. Measurements were taken at the lowest possible chamber background pressure (1.5×10^{-5} torr) and a pressure that was a factor of 2 higher (3.0×10^{-5} torr). In addition to varying the background pressure, the radial magnetic field of the thruster was varied (by a factor of 2) between low- and high-strength configurations. The low-strength configuration produced large-magnitude anode current oscillations, whereas the high-strength configuration produced small current oscillations. Ion axial velocity distribution function peaks were used to approximate ion energy and, in turn, axial electric field strength. Acceleration profiles of the tested thruster operating conditions were compared. High background pressure operation was observed to shift the ion acceleration region upstream in the discharge channel. The width of the velocity distributions correlated strongly to the magnetic field strength. The high magnetic field strength configuration produced narrow velocity distribution functions, whereas the low magnetic field strength configuration led to a broad velocity distribution.

Introduction

ONE of the most significant challenges in ground testing electric propulsion devices is characterizing the effects of background chamber pressure on measured plasma properties. Alteration of the plume due to chamber effects hinders efforts to compare ground test data to numerical simulation and to predict flight characteristics of the thruster. The goal of this study was to examine the effect of background pressure on the ion acceleration mechanism of a medium-power Hall effect thruster by measuring ion velocity distribution functions (VDFs) within the discharge channel. Laser-induced fluorescence (LIF) was used to experimentally measure ion velocity distribution. This optical technique is especially well suited for internal measurements because it is nonintrusive.

Background gas ingested by the thruster affects thruster performance, plume properties, and thruster lifetime. Randolph et al. [1] performed a study on the relationship between these thruster characteristics and background pressure for the SPT-100 Hall effect thruster. Notably, he found that a background pressure of less than 1.3×10^{-5} torr was necessary for accurate charge flux measurements taken within 1.2 m of the thruster due to diffusion of the beam from charge exchange collisions. He also observed that when the background pressure reached a certain threshold (between 3×10^{-5} and 8×10^{-5} torr), the discharge current oscillations became large in amplitude, causing a significant decrease in thruster performance. This decrease in thrust efficiency indicated that the effects of discharge current oscillations outweighed the effects of the thruster using entrained background gas as extra propellant. He attributed these discharge current oscillations to plasma potential instabilities in the near-cathode region or ionization instabilities from increased neutral density in the discharge channel.

Various other experiments have documented facility effects on Hall thrusters. Walker et al. [2] used electrostatic probes 1 m downstream to study background pressure effects on the plume. In another study, Walker and Gallimore [3] examined the effects of background pressure on the performance of a cluster of two Hall thrusters. Their results showed that measured anode efficiency of a 5 kW Hall thruster improved with increased background pressure, contrasting with the findings of Randolph et al. [1] for the SPT-100. Hofer et al. [4] examined performance using a thrust stand for various background pressures. However, little experimental data have been published concerning background pressure effects on the internal ion acceleration of a Hall thruster. Mazouffre et al. [5] used a Fabry–Perót (F–P) interferometry technique to measure axial ion velocity 2 mm upstream of the exit plane of an SPT-100 thruster for two different background pressures. Ion velocity significantly increased in the high-pressure condition, which he attributed to a shift of the acceleration region toward the anode or a narrower acceleration region. This interferometry technique was found to produce results that agreed with LIF data. While nonintrusive, it uses a line-of-sight integration of a xenon ion emission line that necessitates the creation of a simplified plume plasma model to deconvolve velocity distribution. Compared with this technique, LIF measurements have the advantages of better spectral and spacial resolution [5].

Previous internal measurements of ion velocities using LIF have been carried out using a slot cut into the side of a Hall thruster [6,7]. While less intrusive than an internal probe, this modification presumably affects the operation of the thruster. Even if the global effect is small, the local effect may be significant. In the study presented in this paper, internal ion velocity was measured using LIF for an unmodified thruster for various background pressures. This LIF technique for internally interrogating Hall thrusters without the addition of a slot was demonstrated for a 200 W Hall thruster by Hargus and Nakles [8].

Most modern Hall thrusters have acceleration channels with a maximum depth of 1–2 cm. Within a typical channel geometry, it is possible to align collection optics to the probe beam such that limited

Presented as Paper 2008-5101 at the 44th AIAA/ASME/SAE/ASEE Joint Propulsion Conference and Exhibit, Hartford, CT, 21–23 July 2008; received 6 November 2009; revision received 9 October 2010; accepted for publication 14 October 2010.

*Research Engineer, AFRL/RZSS, 1 Ara Road. Member AIAA.
†Research Engineer, AFRL/RZSS, 1 Ara Road. Associate Fellow AIAA.

internal optical access is possible without modification of the Hall thruster. In this experiment, the collection lens was placed 60° off the plume axis. This placement minimizes plume impact since, typically, greater than 95% of a Hall thruster plume ion flux is contained in a 45° half-angle. Using this method, it is possible to probe the internal ion velocity of almost any Hall thruster completely nonintrusively.

In this study, acceleration channel centerline ion velocities were measured for two different chamber background pressures. Measurements were taken at the lowest possible chamber background pressure (1.5×10^{-5} torr) and a pressure that was a factor of two higher. In addition to varying the background pressure, the magnetic field of the discharge channel was switched between two configurations. The radial magnetic field strength was set to low- and high-strength cases, where the high-strength case was a factor of two higher in magnitude. Changing the magnetic field altered the discharge current oscillation magnitude. A dynamic mode, exhibiting large-scale oscillations, was established by using the low-strength radial magnetic field. The high-strength case resulted in small-scale oscillations for a quiescent mode. The goal of this study was to characterize the background pressure effects on the ion acceleration profile at two discharge current oscillatory conditions.

Experimental Apparatus

Xenon Ion Spectroscopy

The LIF signal is a convolution of the species VDF, transition line shape, and laser beam frequency profile. Determination of the VDF from LIF data only requires the deconvolution of the transition line shape and laser beam profile from the raw LIF signal trace. However, previous measurements and analysis have shown that deconvolution is not strictly required to estimate xenon ion VDFs from the raw LIF data in this plasma discharge for this particular xenon transition [9]. The transition is relatively narrow (approximately 600 MHz), and the VDF in the vicinity of the exit plane is sufficiently broad that the fluorescence trace does not require deconvolution of the transition line shape to produce an adequate estimate of the VDF. Not performing the deconvolution further in the plume (e.g., beyond the cathode plane) may introduce uncertainties estimated to be less than 20% [9]. Zeeman splitting is neglected in this analysis due to the broad velocity distributions.

LIF is a convenient diagnostic for the investigation of ion and atomic velocities, as it does not perturb the plasma. LIF measurements are often noise limited and are better suited to determine the most probable velocity than mean velocity. In the skewed, nonsymmetric velocity distributions common to Hall thrusters, the most probable (i.e., peak signal) and statistical mean velocities often differ significantly.

For the results reported here, the $5d[4]_{7/2} - 6p[3]_{5/2}$ electronic transition of Xe II at 834.72 nm is probed. Manzella first used this xenon ion transition to make velocity measurements in a Hall thruster plume [10]. The isotopic and nuclear-spin effects contributing to the hyperfine structure of the $5d[4]_{7/2} - 6p[3]_{5/2}$ xenon ion transition produce a total of 19 isotopic and spin split components. The hyperfine splitting constants that characterize the variations in state energies are only known for a limited set of energy levels. Unfortunately, the 834.72 nm xenon ion transition only has confirmed data on the nuclear-spin splitting constants of the $6p[3]_{5/2}$ upper state [6,11–13]. A convenient feature of this transition is the presence of a relatively strong line originating from the same upper state ($6s[2]_{3/2} - 6p[3]_{5/2}$ transition at 541.9 nm [14], which allows for nonresonant fluorescence collection). Ion velocity is simply determined by measurement of the Doppler shift of the absorbing ions [15].

Test Facility

The LIF measurements were performed in a nonmagnetic stainless steel chamber with a 1.8 m diameter and 3 m length. It had a measured pumping speed of 32,000 liters/s on xenon. Pumping was provided by four single-stage cryogenic panels (single-stage cold heads at 25 K) and one 50 cm two-stage cryogenic pump (12 K). Chamber pressure was measured using a MKS series 423 I-mag cold cathode ionization gauge. The base pressure of the system was measured to be lower than 5.0×10^{-7} torr. Chamber background pressures during thruster operation reported in this study have been corrected from indicated pressure using a gas sensitivity factor of 2.87 for xenon [16]. Chamber background pressure during nominal thruster operation was 1.5×10^{-5} torr. Data were taken at this pressure for a representative low-pressure case. To increase the background pressure for this study, additional xenon gas was flowed into the chamber. The gas was input near the interior wall of the chamber via a gas feedthrough. Figure 1 illustrates the position of the experimental components. The cold cathode ionization gauge used to measure background pressure was located at a radius of approximately 110 cm from the thruster and at the same chamber axial location. The inlet to the pressure gauge was screened to shield the device from electrical currents from the Hall thruster. The gas injection point was located near the chamber ceiling and approximately 100 cm away from the thruster.

For the high-pressure case, xenon was fed into the chamber at a rate of 2.70 mg/s, doubling the background pressure to 3.0×10^{-5} torr. This method of extra gas injection was favored over turning off individual cryopumps to raise the background pressure, because the resulting background pressure was more repeatable and stable. It should be noted that using measurements of chamber background pressure taken near the facility wall is an imperfect method to quantify changes in local pressure in the vicinity of the Hall thruster channel and near plume. The change in this local pressure dominates the changes in the ion acceleration process but, unfortunately, was not possible to measure.

The thruster is mounted on a three-axis orthogonal computer-controlled translation system. The initial alignment of the thruster to the optical measurement location was estimated to be better than 0.5 mm, and the uncertainty of thruster position relative to this initial origin was less than 0.1 mm as it was moved by the translation stage system. Figure 2 shows the Hall thruster and optics mounted within the vacuum chamber, as well as the LIF apparatus. The laser is a tunable diode laser. It is capable of tuning approximately ±50 GHz about a center wavelength of 834.72 nm. The 6 mW beam is passed through a Faraday isolator to eliminate feedback to the laser. The laser beam then passes through several beam pickoffs until it is focused by a lens and enters the vacuum chamber through a window. The probe beam is chopped at a frequency by an optical chopper (Ch2 at 2.8 kHz) for phase-sensitive detection of the fluorescence signal.

The two wedge beam pickoffs (BS denotes beam splitter) shown in Fig. 2 provide portions of the beam for diagnostic purposes. The first beam pickoff directs a beam to a photodiode detector (D1) used to provide constant power feedback to the laser. The second beam is divided into two equal components by a 50–50 cube beam splitter.

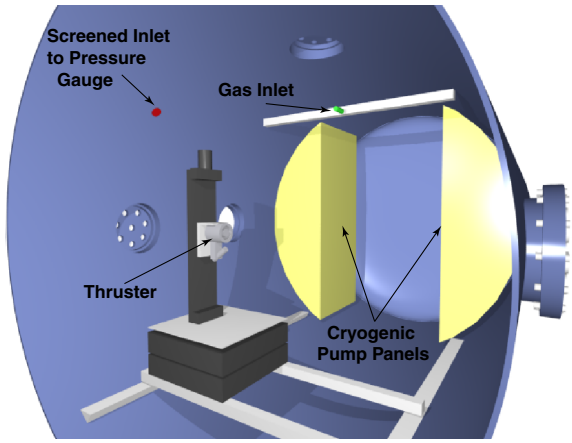

Fig. 1 Diagram of chamber interior showing the relative position of the thruster, cold cathode ionization gauge, gas flow inlet, and cryogenic pump panels. Note that experimental optics are not shown in this figure.

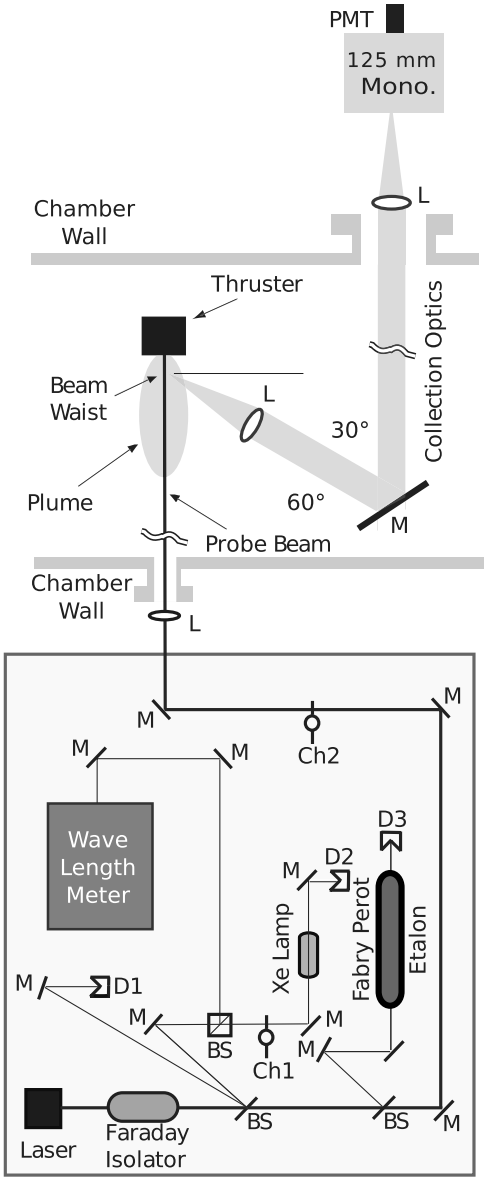

Fig. 2 Diagram of laser optical train and collection optics.

The first component is directed to a wavemeter used to monitor absolute wavelength. The second component is sent through an optical chopper (Ch1 at 1.4 kHz) and through a low-pressure xenon hollow cathode discharge lamp. The lamp provides a stationary absorption reference for the determination of the Doppler shift. Unfortunately, there is no detectable population of the ionic xenon $5d[4]_{7/2}$ state. However, there is a nearby (estimated to be 18.1 GHz distant) neutral xenon $6s'[1/2]_1 - 6p'[3/2]_2$ transition at 834.68 nm [17,18]. The second pickoff sends a beam to a 300 MHz free spectral range F–P etalon that provides high-resolution frequency monitoring of the wavelength interval swept during a laser scan.

The fluorescence collection optics are also shown in Fig. 2. The fluorescence is collected by a 75-mm-diam 300 mm focal length lens within the chamber, oriented 60° from the probe beam axis. The collimated fluorescence signal is directed through a window in the chamber sidewall to a similar lens that focuses the collected fluorescence onto the entrance slit of a 125 mm focal length monochrometer with a photomultiplier tube (PMT). Because of the 1:1 magnification of the collection optics, the spatial resolution of the measurements is determined by the geometry of the entrance slit (0.7 mm width and 1.5 mm height), as well as the submillimeter diameter of the probe beam. This apparatus allows for limited probing of the interior acceleration channel of Hall thrusters with relatively shallow acceleration channels. Measurements show that this combination of apparatus and laser power are within the linear fluorescence regime [15].

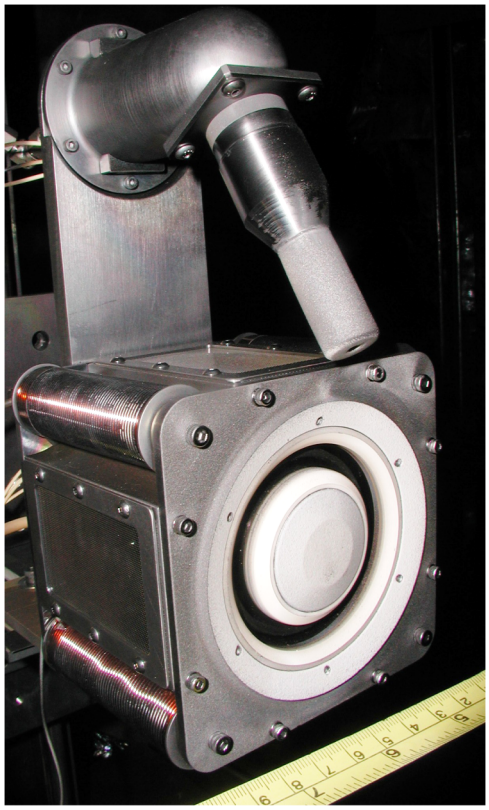

Fig. 3 Photograph of Busek BHT-600 Hall effect thruster used in study.

Hall Effect Thruster

The Hall thruster used in this study is the rectangular 600 W Busek Company BHT-600 Hall thruster with a 3.2 mm hollow cathode. A photograph of the thruster is shown in Fig. 3. This thruster has a conventional five-magnetic-core (one inner and four outer) magnetic circuit. The acceleration channel of the thruster has a 32 mm outer radius and a 24 mm inner radius. The acceleration channel has a depth of approximately 10 mm between the geometrical exit plane and the furthest forward extent of the anode. The thruster has been extensively characterized to have a thrust of 39 mN with a specific impulse of 1530 s, yielding an efficiency of approximately 50% at the nominal conditions specified in Table 1.

Varying the magnetic field by changing the applied current to the four series connected outer magnetic cores and the central core allowed for the examination of two distinct anode current oscillatory conditions. The two oscillatory conditions were studied at each background pressure condition. The high magnetic field configuration had twice the radial magnetic field strength as the low magnetic field case. Despite the change in field strength, the shape of the radial field profile remained similar. Figure 4 shows the normalized radial field profiles along the acceleration channel centerline calculated using a commercial software simulation package.

Table 1 Nominal BHT-600 Hall thruster operating conditions

Parameter	Value
Anode flow	2.45 mg/s Xe
Cathode flow	197 μg/s Xe
Anode potential	300 V
Anode current	2.16 A
Keeper current	0.5 A
Heater current	3.0 A

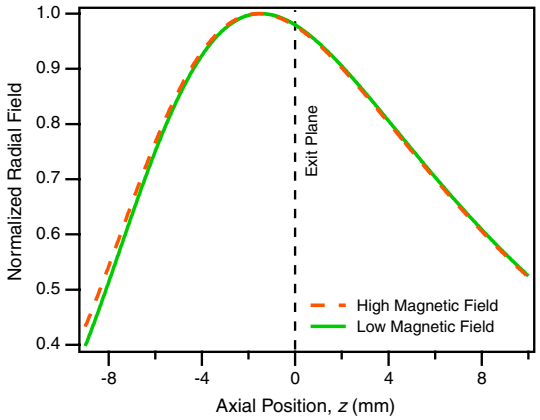

Fig. 4 Normalized radial magnetic field strength along acceleration channel centerline. Radial field strength is a factor of two greater in the high case than in the low case. However, the profile of the radial field strength is nearly identical between both cases.

Figure 5 shows a cutaway view of the near-field geometry of the Hall thruster. The locations of the central magnetic poles and edges of the acceleration channel are indicated, as is the position of the cathode. The Cartesian coordinate system and origin used in these measurements are also shown in Fig. 5, with the positive x axis going into the page. The origin is at the center of the thruster face due to the ease and repeatability with which this position could be located. The cathode orifice plane is located at $z = 20$ mm. All measurements presented in this work lie on the $x = 0$ mm and $y = +28$ mm line. This corresponds to the acceleration channel centerline.

Results and Discussion

Anode Current Oscillations

The variation of magnetic field strength resulted in two distinct anode current oscillatory regimes. Figure 6 displays the anode current fluctuations with time, along with the corresponding frequency spectrum. The high magnetic field case produced a quiescent mode where the oscillations were small relative to the mean current. The standard deviation of anode current was less than 10% of the mean. The oscillations appear to be broadly spread below 100 kHz. A dynamic mode appeared for the low magnetic field case where the amplitude of the anode current oscillations was large. Here, the discharge current standard deviation was greater than 34% of the mean. This mode exhibited a strong peak frequency of 44 kHz that, which in the time domain plots is seen as a more coherent sinusoid oscillation that dominated the anode current. The low magnetic field case also differed by displaying a prominent harmonic. Despite the varying oscillation patterns, the mean current was similar among the four different combinations of magnetic field and background pressure (only varying a few percent). These oscillatory modes appear to be consistent with the breathing mode oscillation that has been described by Choueiri [19]. The breathing mode plasma oscillation has been characterized as a discharge current instability that manifests itself as periodic axial translation of the ionization zone accompanied by the local ion accelerating plasma potential.

Magnetic field strength was the main factor in the oscillatory behavior of the anode current; however, background pressure variation also produced measurable variations. In the high magnetic field case, high chamber pressure was observed to increase the magnitude of the anode current oscillations, doubling the standard deviation. The peak oscillation frequency also increased slightly from 43.1 to 44.5 kHz. The effect of higher chamber pressure was less pronounced for the low magnetic field case. Here, the standard deviation of the anode current only increased by 12%. However, the frequency spectrum displayed an increase in the presence of high-frequency oscillations near the harmonic frequency.

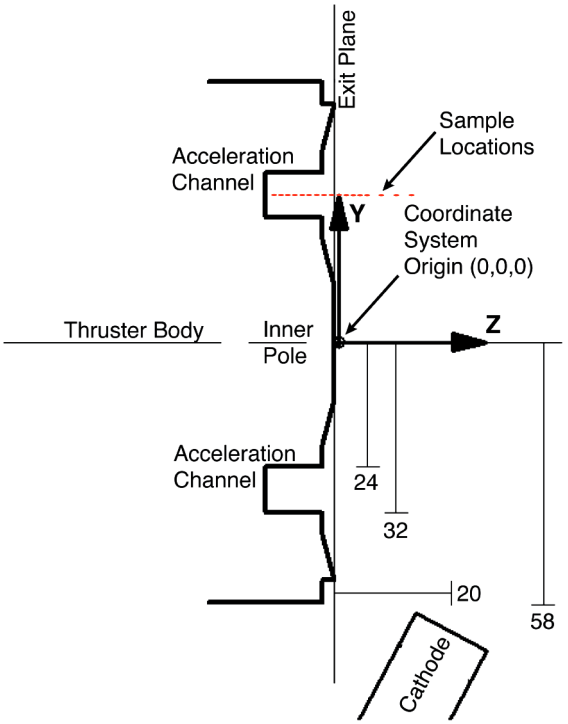

Fig. 5 Cross section of the BHT-600 Hall thruster showing the coordinate system for LIF measurements and sample measurement locations. (Dimensions are in millimeters.)

Ion Velocity Distribution

Ion VDFs were measured in the $y - z$ plane ($x = 0$) along the centerline of the acceleration channel ($y = 28$ mm). The measurement locations ranged from just downstream of the anode ($z = -9$ mm) to 10 mm downstream of the exit plane ($z = 10$ mm).

Figure 7 displays the trend of the VDFs throughout the acceleration region for all four cases. The most apparent effect of high-pressure operation is that ions have a higher velocity at locations inside the acceleration channel for both magnetic field cases. Beyond the exit plane, the low-pressure-case ion velocity appears to catch up with the velocity at high pressure. By 10 mm beyond the exit plane, the velocity peak locations for both pressure cases are nearly equal. Increased electron cross-field mobility due to neutral collisions may be responsible for expanding the potential gradient further upstream in the high-pressure condition, thus initiating ion acceleration closer to the anode compared with low pressure operation.

Another effect is a perceptible variation in the width of the velocity distribution. An increase in width is prevalent in the deep interior for both magnetic field strength cases at high pressure. However, in the low magnetic field strength case, the high background pressure VDFs are actually less broadened beyond the exit plane than the low-pressure case. This may indicate that the high-pressure reduces the severity of external plasma oscillations, as kinematic compression narrows the velocity distributions during the external acceleration between the exit plane and cathode plane.

Inducing anode oscillations by varying the magnetic field distinctly affects the broadness of the velocity distributions. At both background pressure conditions, the introduction of strong anode current oscillations results in much broader velocity distributions. This broadness is presumably due to the larger oscillations in the local plasma potential and ionization location. These oscillations take place on a much smaller timescale than the relatively long LIF integration times (typically 4–7 min), thus resulting in a time-averaged LIF trace, which incorporates a greater variation in velocity compared with the quiescent mode derived from the high magnetic field setting. More interesting, the peak and mean velocities appear to be higher for the low magnetic field cases at $z = 10$ mm, perhaps indicating that the highly oscillatory cases are more efficient at recovering the applied discharge potential.

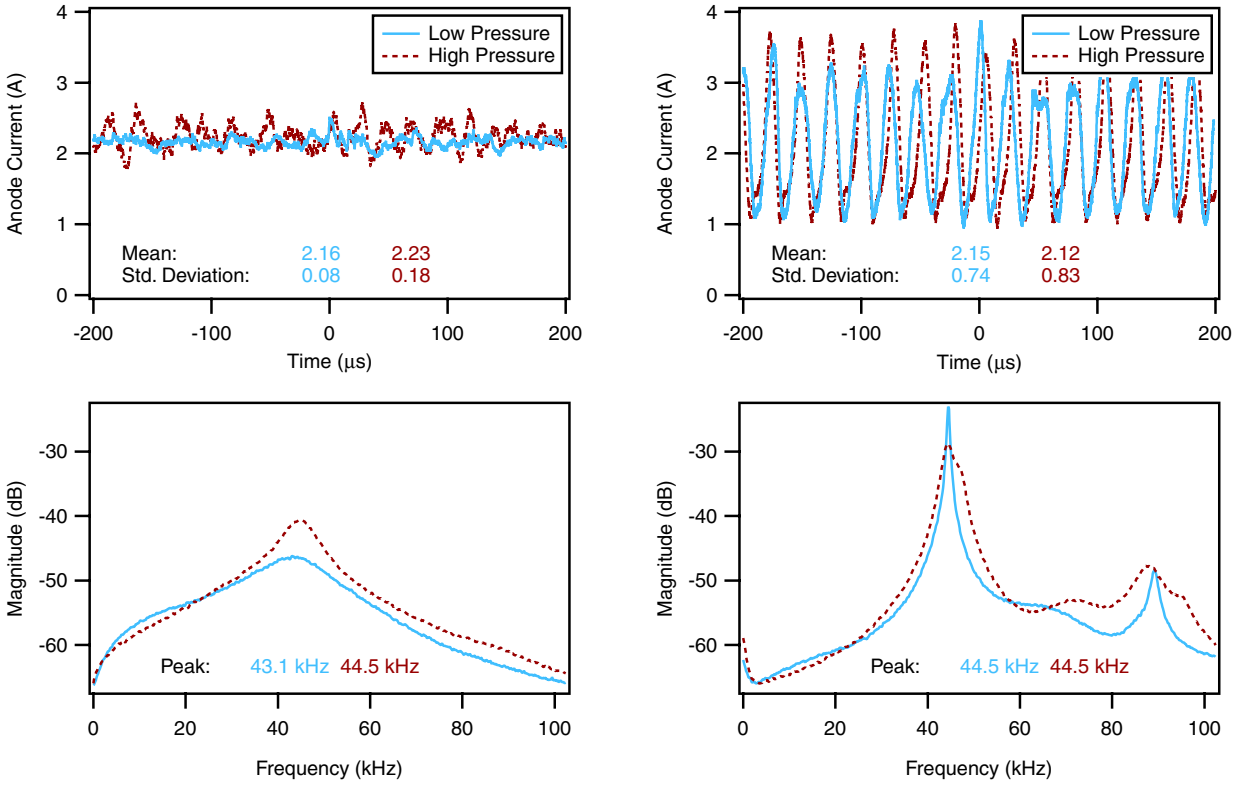

a) High magnetic field case **b) Low magnetic field case**

Fig. 6 Anode current time and frequency domain behavior for four experimental cases. Frequency spectra are plotted in arbitrary units of magnitude.

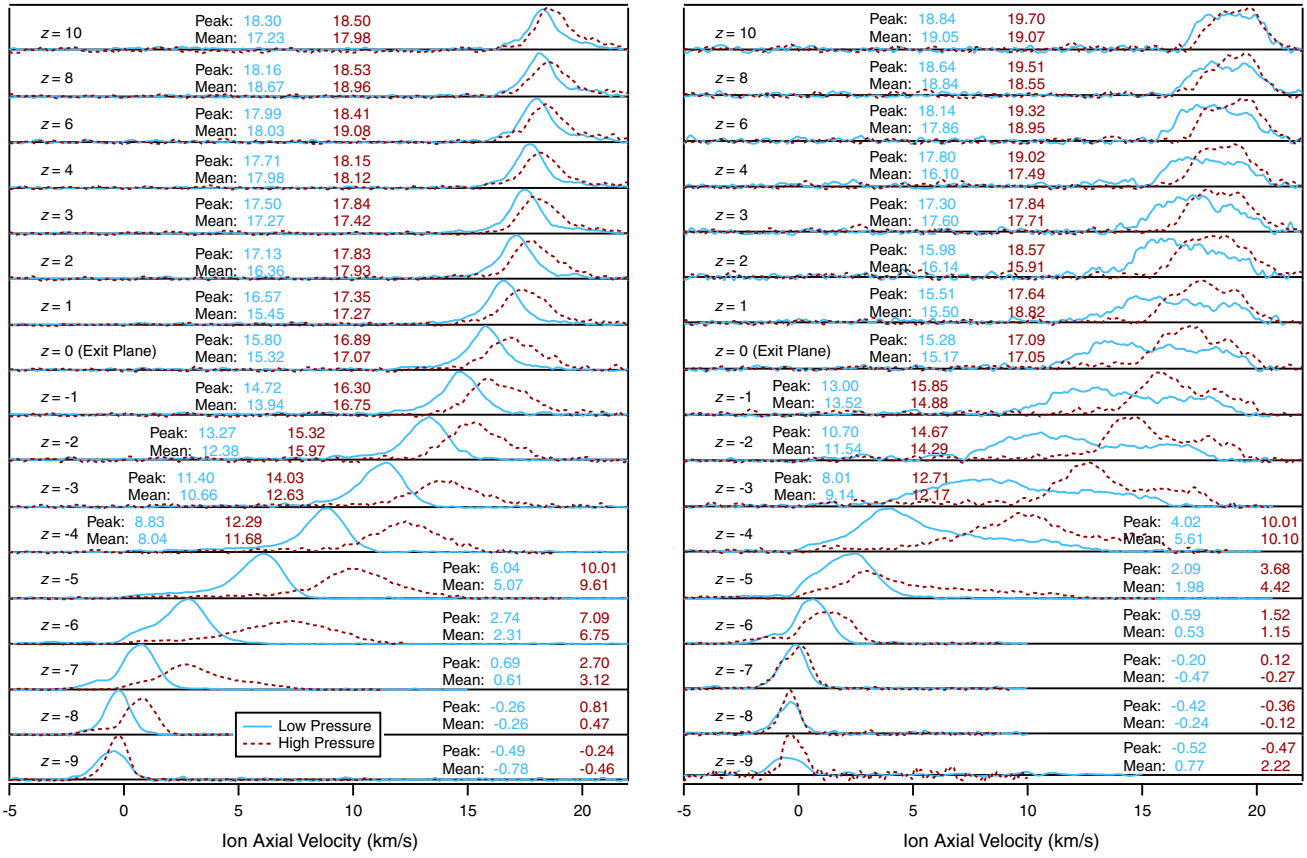

a) High magnetic field case **b) Low magnetic field case**

Fig. 7 Axial ion VDFs along acceleration channel centerline (units: axial position; z: mm; and peak and mean velocity: km/s). Peaks are area normalized to unity.

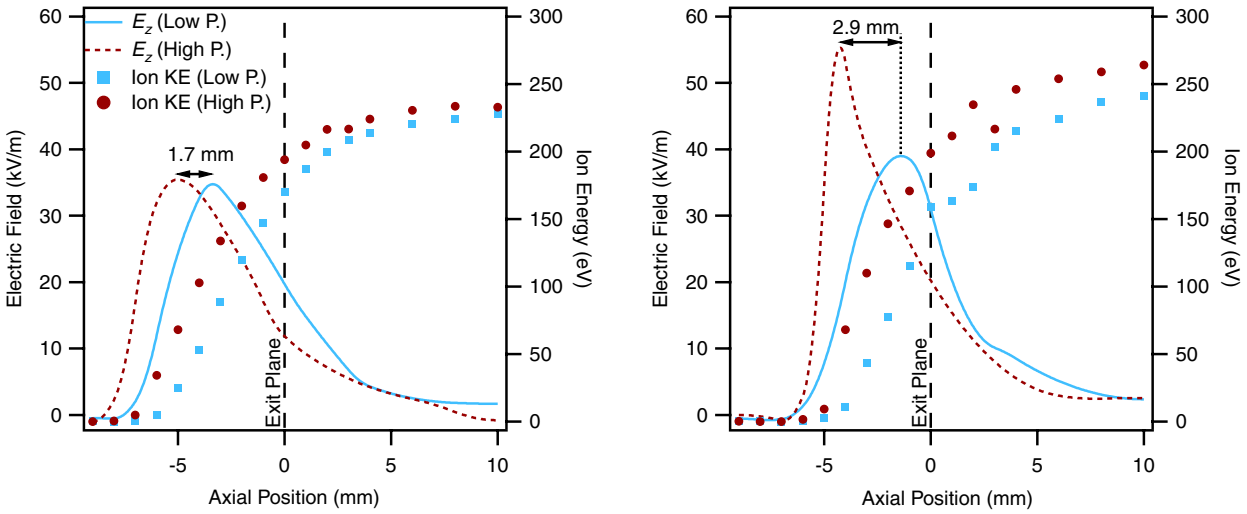

a) High magnetic field case **b) Low magnetic field case**

Fig. 8 Ion energy distribution peak profile and derived axial electric field strength (KE denotes kinetic energy). Electric field strength was approximated by differentiating ion energy peak with respect to z. (Note that ion energy peak function was smoothed before differentiation.)

Axial electric field strength throughout the measurement region was approximated using the peak velocity of the LIF traces along the z direction. Plasma potential was estimated from the kinetic energy of the ions and then differentiated with respect to axial distance. The ion peak velocity trend was smoothed before differentiation to account for ambiguity in peak location from the velocity uncertainties.

Figure 8a shows that, in the high magnetic field configuration, the peak of the electric field is shifted almost 2 mm upstream for the high-pressure case, but it retains a similar shape to the low-pressure case. The reason for this upstream shift is not precisely known, but it has been observed previously when propellant flow rates were increased [8]. This shift in the electric field may be due to greater neutral ingestion, which provides a greater probability of electron collisions. A greater collision frequency would raise the classical electron conductivity, and perhaps push the electric field farther into the acceleration channel.

Figure 8b shows that the high-pressure electric field peak shifts upstream nearly 3 mm in the low magnetic field configuration. However, in contrast to the high magnetic field configuration, the electric field profile changes significantly with pressure. The peak axial electric field increases by more than 30%. The peak of the electric field is moved upstream to near $z = -4$, which corresponds to the location of maximum VDF width. This is consistent with the supposition that the increased oscillations cause increased electron transport due to plasma turbulence: in this case, in the form of axial plasma oscillations.

It appears that a modest increase in background pressure (two times) produces an upstream shift in the location of ion acceleration within the Hall effect thruster channel and affects the electric field profile shape significantly when axial disturbances are present within the discharge. One note of caution should be sounded in this analysis of the electric fields. The fields shown in Fig. 8b are not only calculated using the most probable velocity to calculate the most probable ion energy but, by their very nature, are time averaged. It is almost certain that the plasma potential within the acceleration channel is, in fact, oscillating at high frequencies, and the instantaneous electric field is, in fact, very different than the time-averaged derivation from the LIF measurements. There is value in the time-averaged quantity from the perspective of studying thruster erosion, predicting lifetime and assessing thruster performance. However, it must be remembered that these LIF data cannot be used to study instantaneous plume properties.

Conclusions

Increasing background pressure shifted the ion acceleration region upstream and led to VDF broadening, particularly at locations inside the acceleration channel. The low magnetic field configuration led to increased discharge oscillations and had the effect of increasing the VDF width throughout the measurement location range. This is likely an indication of the oscillation of the thruster breathing mode, which produces a dithering of the local plasma potential and thus affects the local instantaneous ion velocities. Increasing the background pressure seems to increase this effect within the thruster, but it damps this effect in the near plume.

At the high magnetic field setting (quiescent mode), the axial electric field profile shifts upstream for the high-pressure case while retaining its basic profile. However, for the low magnetic field setting (dynamic mode), a steeper profile shape accompanies the upstream shift of the axial electric field profile when background pressure increases.

More interesting, the peak ion velocity (and hence energy) at the downstream extent of measurement region is higher for the more oscillatory cases. This includes the oscillations induced by raising the background pressure. The extent of any performance gain or loss has not yet been characterized. However, it is interesting to note the introduction of oscillations moves the time-averaged peak electric field downstream and increases the peak value. It is not yet known what the tradeoff is with respect to lifetime between moving the peak electric field downstream and producing higher energy ions deep within the acceleration channel due to the oscillations in the local plasma potential.

Background pressure effects on thruster operation appear to be a complex issue and, at lower background pressures, are not simply an addition to the discharge current due to ingestion. The effect of background pressure changes the acceleration profile and the oscillatory behavior of the thruster. This has serious implications for the understanding of ground-based testing of Hall thrusters. In previous studies, Hall thruster researchers have proposed background pressure criteria for far-field plume and performance measurements. The measurements in this work suggest that background pressure criteria should also be established for internal and near-field plasma measurements of Hall effect thrusters. Hall thruster operation with a facility operating pressure of 3.0×10^{-5} torr exhibited significant background pressure effects on internal ion velocity. The required background pressure for adequately minimizing chamber effects is still unknown and requires further investigation.

Acknowledgments

The authors would like to thank Garrett Reed of the U.S. Air Force Research Laboratory for his assistance with the laser-induced fluorescence data acquisition system and Bruce Pote and Rachel

Tedrake of Busek Company, Inc., for their assistance in the magnetic field characterization of the BHT-600.

References

[1] Randolph, T., Kim, V., Kaufman, H., Korzubusky, K., Zhurin, V., and Day, M., "Facility Effects on Stationary Plasma Thruster Testing," 23rd International Electric Propulsion Conference, Seattle, WA, IEPC Paper 93-93, Electric Rocket Propulsion Soc., Fairview Park, OH, Sept. 1993.

[2] Walker, M. L. R., Victor, A. L., Hofer, R. R., and Gallimore, A. D., "Effect of Backpressure on Ion Current Density Measurements in Hall Thruster Plumes," *Journal of Propulsion and Power*, Vol. 21, No. 3, May–June 2005, pp. 408–415. doi:10.2514/1.7713

[3] Walker, M. L. R., and Gallimore, A. D., "Performance Characteristics of a Cluster of 5-kW Laboratory Hall Thrusters," *Journal of Propulsion and Power*, Vol. 23, No. 1, 2007, pp. 35–43. doi:10.2514/1.19752

[4] Hofer, R. R., Peterson, P. Y., and Gallimore, A. D., "Characterizing Vacuum Facility Backpressure Effects on the Performance of a Hall Thruster," 27th International Electric Propulsion Conference, Pasadena, CA, IEPC Paper 01-045, Electric Rocket Propulsion Soc., Fairview Park, OH, Oct. 2001.

[5] Mazouffre, S., Pagnon, D., and Bonnet, J., "Two Ways to Evaluate the Xe^+ Ion Flow in a Hall Effect Thruster: LIF Spectroscopy and Fabry–Perót Interferometry," 40th AIAA/ASME/SAE/ASEE Joint Propulsion Conference and Exhibit, Fort Lauderdale, FL, AIAA Paper 2004-3949, 2004.

[6] Hargus, W. A., Jr., and Cappelli, M. A., "Laser-Induced Fluorescence Measurements of Velocity Within a Hall Discharge," *Applied Physics B: Lasers and Optics*, Vol. 72, No. 8, June 2001, pp. 961–969. doi:10.1007/s003400100589

[7] Dorval, N., Bonnet, J., Marque, J., Rosencher, E., Chable, S., Rogier, F., and Lasgorceix, P., "Determination of the Ionization and Acceleration Zones in a Stationary Plasma Thruster by Optical Spectroscopy Study: Experiments and model," *Journal of Applied Physics*, Vol. 91, No. 8, April 2002, pp. 4811–4817. doi:10.1063/1.1458053

[8] Hargus, W. A., Jr., and Nakles, M. R., "Ion Velocity Measurements Within the Acceleration Channel of a Low-Power Hall Thruster," *IEEE Transactions on Plasma Science*, Vol. 36, No. 5, Oct. 2008, pp. 1989–1997. doi:10.1109/TPS.2008.2003967

[9] Hargus, W. A., Jr., and Nakles, M. R., "Evolution of the Ion Velocity Distribution in the Near Field of the BHT-200-X3 Hall Thruster," 42nd Joint Propulsion Conference and Exhibit, AIAA Paper 2006-4991, July 2006.

[10] Manzella, D. H., "Stationary Plasma Thruster Ion Velocity Distribution," 30th Joint Propulsion Conference and Exhibit, AIAA Paper 1994-3141, June 1994.

[11] Geisen, H., Krumpelmann, T., Neuschafer, D., and Ottinger, C., "Hyperne Splitting Measurements on the 6265 Angstrom and 6507 Angstrom Lines of Seven Xe Isotopes by LIF on a Beam of Metastable $Xe(^3P_{0,3})$ Atoms," *Physics Letters A*, Vol. 130, Nos. 4–5, July 1988, pp. 299–309. doi:10.1016/0375-9601(88)90614-7

[12] Fischer, W., Huhnermann, H., Kromer, G., and Schafer, H. J., "Isotope Shifts in the Atomic Spectrum of Xenon and Nuclear Deformation Effects," *Zeitschrift für Physik*, Vol. 270, No. 2, Jan. 1974, pp. 113–120. doi:10.1007/BF01677442

[13] Bronstrom, L., Kastberg, A., Lidberg, J., and Mannervik, S., "Hyperfine-Structure Measurements in Xe II," *Physical Review A*, Vol. 53, No. 1, Jan. 1996, pp. 109–112. doi:10.1103/PhysRevA.53.109

[14] Hansen, J. E., and Persson, W., "Revised Analysis of Singly Ionized Xenon, Xe II," *Physica Scripta*, Vol. 36, No. 4, 1987, pp. 602–643. doi:10.1088/0031-8949/36/4/005

[15] Demtroder, W., *Laser Spectroscopy: Basic Concepts and Instrumentation*, Springer-Verlag, New York, 1996, pp. 384–388.

[16] Summers, R., "Empirical Observations on the Sensitivity of Hot Cathode Ionization Type Vacuum Gages," NASA, TN D-5285, 1969.

[17] Miller, M. H., and Roig, R. A., "Transition Probabilities of Xe I and Xe II," *Physical Review A*, Vol. 8, No. 1, July 1973, pp. 480–486. doi:10.1103/PhysRevA.8.480

[18] Moore, C. E., *Atomic Energy Levels*, Vol. 2, National Bureau of Standards, Bethesda, MD, 1958, pp. 113–123.

[19] Choueiri, E., "Plasma Oscillations in Hall Thrusters," *Physics of Plasmas*, Vol. 8, No. 4, April 2001, pp. 1411–1426. doi:10.1063/1.1354644

A. Gallimore
Associate Editor